Vapor-Phase Self-Assembled Monolayers for Anti-Stiction Applications in MEMS

Yan Xin Zhuang, Ole Hansen, Thomas Knieling, Christian Wang, Pirmin Rombach, Walter Lang, Wolfgang Benecke, Markus Kehlenbeck, and Jörn Koblitz

Abstract—We have investigated the anti-stiction performance of self-assembled monolayers (SAMs) that were grown in vapor phase from six different organosilane precursors: $CF_3(CF_2)_5(CH_2)_2SiCl_3$ (FOTS), $CF_3(CF_2)_5(CH_2)_2Si(OC_2H_5)_3$ (FOTES), $CF_3(CF_2)_5(CH_2)_2Si(CH_3)Cl_2$ (FOMDS), $CF_3(CF_2)_5(CH_2)_2Si(CH_3)_2Cl$ (FOMMS), $CF_3(CF_2)_7(CH_2)_2SiCl_3$ (FDTS), and $CH_3(CH_2)_{17}(CH_2)_2SiCl_3$ (OTS). The SAM coatings that were grown on silicon substrates were characterized with respect to static contact angle, surface energy, roughness, nanoscale adhesive force, nanoscale friction force, and thermal stability. The best overall anti-stiction performance was achieved using FDTS as precursor for the SAM growth, but all coatings show good potential for solving in-use stiction problems in microelectromechanical systems devices. [2007-0062]

Index Terms—Adhesion, anti-stiction, friction, self-assembled monolayer (SAM), thermal stability, vapor phase.

I. INTRODUCTION

WITH miniaturization of microelectromechanical systems (MEMS) and nanoelectromechanical systems (NEMS) devices, various surface forces such as capillary, hydrogen bonding, electrostatic, and van der Waals forces become dominant over gravity and inertia. Stiction occurs when the internal restoring forces of micro/nanostructures cannot overcome the attractive interfacial forces. Stiction can occur either during fabrication (release stiction) and/or in applications (in-use stiction). Stiction is a serious problem during fabrication and in applications of silicon microstructures since it will significantly affect the reliability, long-term stability, efficiency, and durability of the devices [1]–[4]. Release stiction occurs in wet sacrificial layer removal processes, mainly due to cap-

illary forces. Several techniques have been developed for the elimination of release stiction problems, such as dry sacrificial layer release etching [5] or special drying processes, such as freeze sublimation [6] and supercritical CO_2 drying [7]. However, in-use-stiction-related failure remains a major problem and will be increasingly important with miniaturization toward nanoscale structures. An efficient way to avoid or reduce in-use stiction is to deposit a thin layer of low-surface-energy material on the surfaces of the microstructures. Among various surface coatings and modification techniques, self-assembled monolayers (SAMs) that are grown from organosilanes are promising candidates for anti-stiction coatings due to their good bonding strength, low surface energy, low friction forces, and good thermal stability. It is well known that the application of hydrocarbon- or fluorocarbon-based SAMs can significantly reduce stiction and adhesion in micro/nanostructures. Both liquid-phase processes [8]–[14] and vapor-phase processes [15]–[23] have been developed for depositing organosilane SAM films on MEMS/NEMS devices.

Liquid-phase processes were the first processes that were investigated for producing quality SAM films to reduce stiction in microstructures. The most commonly used precursors are chlorosilane based [8]–[14], such as octadecyltrichlorosilane (OTS), 1H, 1H, 2H, 2H-perfluorocdecyltrichlorosilane (FDTS), and dichlorodimethylsilane (DDMS). Liquid-phase SAMs that are grown in well-controlled conditions have shown good anti-stiction properties. In liquid-phase SAM growth processes, the release stiction problems are reduced or eliminated if the microstructures are kept wetted during the full release etching and SAM coating process. However, SAM coatings that are grown in liquid phase have significant drawbacks, such as complicated process control, the generation of large amounts of contaminated effluents, insufficient stiction prevention, and high production costs [14]. Vapor-phase processes can eliminate some of the problems that are seen in liquid-based processes [16], [20], [23], [24] and thereby attract strong attention. In vapor-phase processes, the precursor chemistry is easily controlled, efficient mass transport ensures coating of high-aspect-ratio structures, and self-limiting surface reactions lead to conformal monolayer coverage [24]. It has been shown that the performance of SAM coatings that are grown in vapor phase is comparable or superior to SAMs that are grown in liquid phase [16], [23]. Moreover, vapor-phase processes have better reproducibility and can be easily adapted to industrial requirements. In vapor-phase SAM coating processes, the release stiction problems must be solved using special release etching or drying techniques as previously mentioned. Until
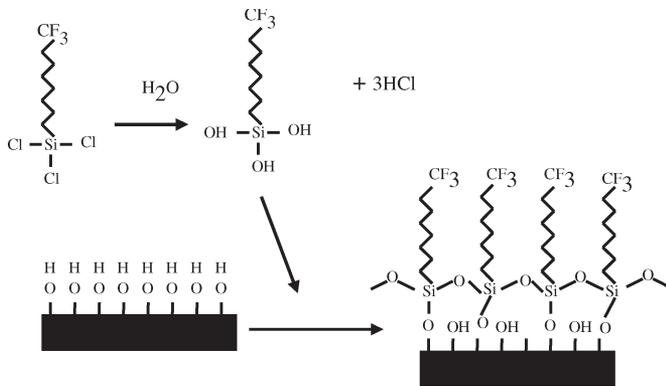
Fig. 1. Formation mechanism of SAM on the hydroxylized silicon substrate.

now, only FOTS, FDTS, and DDMS have been frequently used as precursors in vapor-phase SAM processes [16], [20]–[23]. However, a wide variety of anti-stiction precursors are available. Some of them may show better performance such as reduced HCl evolution without significant loss in thermal stability. Therefore, we decided to conduct a comparative study of several alternative precursors for vapor-phase processes and compare their performance to the performance of FDTS and OTS.

Growth of SAM coatings from silanes proceeds through two steps, as shown in Fig. 1. In the first step, the active head group reacts with H_2O vapor to form hydroxyle groups, which, in the second step, anchor the chains of the molecules to hydroxyle groups on the substrate surface. In the case of multifunctional silanes also lateral bonds between the molecules can be formed through reaction between the hydroxyle groups. The SAM coating quality depends on the process parameters and the nature of the precursors. In vapor-phase processes, the water vapor concentration in the reaction chamber must be carefully controlled. Otherwise, low-coverage SAM coatings can be formed due to insufficient water content or a coating with many aggregations because of excess water.

Chlorosilanes are very reactive and have been widely used in anti-stiction SAM coatings. However, the coating process will produce HCl as a byproduct, which might be very harmful for some metallized devices. Therefore, triethoxysilane was tested in this paper, even though it has lower reactivity than chlorosilane. The number of functional groups is also an important factor in determining SAM coating quality. Trifunctional silanes are able to form a monolayer where the molecules are linked together by strong Si–O–Si bonds [25]. This results in high stability against external impact, particularly, against thermal influence. Trichlorosilane is most reactive; thus, the reaction time is expected to be comparatively low. However, trichlorosilane has high tendency to polymerize in the presence of too much water, and it will produce larger amounts of HCl than monochlorosilane. Monochlorosilane is only able to form covalent bonds, while dichlorosilane forms covalent bonds or vertical polymerizations. The layers resulting from mono- or dichlorosilanes are expected to be less tightly packed than the methyl groups; the increased risk of vertical polymerization on the other hand can increase the roughness of the films that were grown from di- and, particularly, trichorosilanes. Finally, the

thermal stability is expected to be weaker for layers that were grown from mono- or dichlorosilane than for layers that were grown from trichlorosilane.

Therefore, we have investigated the application of six reactive organosilanes to modify the surface properties and to improve the surface hydrophobization of silicon substrates. The six chemicals have two different surface terminal groups (Trifluoromethyl $-CF_3$ and Methyl $-CH_3$), three different spacer chains ($-(CF_2)_7(CH_2)_2-$, $-(CF_2)_5(CH_2)_2-$, and $-(CH_2)_{17}-$), and four different surface active head groups (Trichlorosilane $-SiCl_3$, Methyldichlorosilane $-Si(CH_3)Cl_2$, Dimethylchlorosilane $-Si(CH_3)_2Cl$, and Triethoxysilane $-Si(OC_2H_5)_3$), which react with the pretreated surface to form a strong chemical bond. The precursors that were used are $CF_3(CF_2)_7(CH_2)_2SiCl_3$ (FDTS), $CF_3(CF_2)_5(CH_2)_2SiCl_3$ (FOTS), $CF_3(CF_2)_5(CH_2)_2Si(OC_2H_5)_3$ (FOTES), $CF_3(CF_2)_5(CH_2)_2Si(CH_3)Cl_2$ (FOMDS), $CF_3(CF_2)_5(CH_2)_2Si(CH_3)_2Cl$ (FOMMS), and $CH_3(CH_2)_{17}SiCl_3$ (OTS). Among the six molecules, FOTS, FOMDS, and FOMMS are different in the number of functional groups on the active head group ($-Cl$ here), FDTS and FOTS have different lengths of the fluorocarbon spacer chain, and FOTS and FOTES have different functional groups on the trifunctional head group ($-Cl$ for FOTS and $-OC_2H_5$ for FOTES).

We expected that the effect of the surface terminal group, chain length, chain type, and functionality and type of the active head group of the precursors would show in the performance of the resulting SAM coatings. The SAM coatings were deposited onto the silicon substrate in a vapor-phase process and subsequently characterized by several techniques. The contact angle, surface energy, roughness, water condensation figure, nanoscale adhesive force, nanoscale friction force, and thermal stability were measured and compared. Finally, the net performance as an anti-stiction coating is discussed.

II. Experimental Technique

The vapor-phase coating process has been carried out in a vapor-phase coating setup that was described in detail in [26], where process pressures down to 0.2 mbar and process temperatures between 20 °C and 300 °C can be reached. Before the actual coating process, a pretreatment step was applied in order to terminate the monosilicon wafer surface with OH groups. The pretreatment step comprises a treatment in an O_2 plasma for 30 min in a Tepla barrel reactor at 100 W, a Piranha clean (H_2O_2 : H_2SO_4, 1 : 1) at 100 °C for 15 min, followed by a quick dump rinse in DI water, and a smooth nitrogen brush drying at low temperature. After the pretreatment process, the silicon wafer is terminated with OH groups and covered with a thin water film, which is necessary during the SAM reaction. Then, the $4''$ silicon wafer was loaded into the process chamber together with Petri dishes containing precursors. After heating and a reduction of the pressure to 0.2 mbar, the silane precursor evaporates into the inner process chamber space and creates a saturated atmosphere consisting of the coating molecules, which react on the substrate and form a SAM coating. Unfortunately, in the deposition setup that was used, the water

amount cannot be precisely controlled and measured. However, by carefully controlling the process and the time delay between the pretreatment and silanization, high-quality SAM coatings have been archived. Following the deposition, the coating was characterized by water contact angle measurements, followed by a detailed examination using an atomic force microscope (AFM). Only coatings without aggregations were used in subsequent nanoscale adhesive and friction force measurements, and thermal stability tests.

The contact angle measurements were performed using a contact angle meter DSA10 from Krüss GmbH that is equipped with an automatic dispensing system for four liquids and a frame grabber. Static contact angles were used to evaluate the SAM coatings. The static contact angle values were taken 5 s after deposition of the droplets on the surface to allow droplet relaxation. At least ten measurements were performed for each droplet. The static contact angle values that were reported are the average of measurements on at least ten droplets. The surface energy of coatings was calculated from static contact angles of water, diiodomethane, and ethylene glycol according to the Owens–Wendt–Rabel–Kaelble method, as described in [27].

The AFM images that were used for characterization were taken in tapping mode using commercial silicon tips on a commercial AFM system (NanoMan, Digital Instrument, Santa Barbara, CA). The images were analyzed using the software Nanoscope 6.12 (Digital Instrument, Santa Barbara, CA). The average roughness R_a, root-mean-square roughness R_{rms}, and maximum peak roughness R_{max} were extracted from the images and used for characterization. All roughness data were obtained from a 5×5 μm^2 scanning area. AFM measurements have been performed at different positions across the wafers to observe if aggregations were present on the coatings and to characterize the coating homogeneity.

In some cases, water condensation figures were also obtained in order to study the coating homogeneity. For this purpose, the sample to be studied was loaded into a transparent box together with a droplet of water and cooled down using a Peltier element. After cooling the sample, water condensates on the surface, and the resulting condensation figures were recorded using a charge-coupled device camera that is mounted on a microscope.

Nanoscale adhesion and friction force measurements were carried out using a commercial AFM system (NanoMan, Digital Instrument, Santa Barbara, CA) that is operated under ambient conditions at 22 °C and 45%–55% relative humidity. Square pyramidal Si_3N_4 tips with a nominal tip radius in the range of 20–60 nm that were mounted on gold-coated Si_3N_4 cantilevers with a nominal spring constant of 0.32 N/m (Digital Instrument, Santa Barbara, CA) were used in this paper. The adhesive force measurements were carried out in the force calibration mode. In this mode, a force distance curve is obtained by exciting the piezotube in the Z-direction using a triangular excitation waveform. This excitation waveform forces the cantilever tip to move up and down in the Z-direction relative to the stationary sample; the resulting cantilever deflection signal is simultaneously monitored using a photodiode. A typical force distance curve, i.e., a plot of the cantilever deflection signal as a function of the voltage that is applied to the piezotube and the resulting
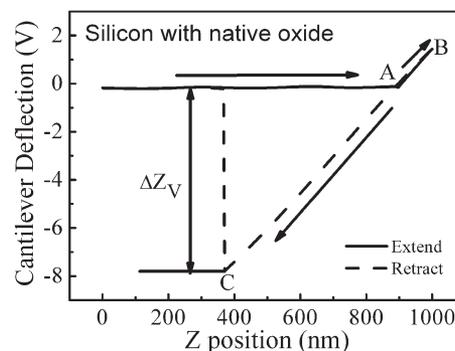

Fig. 2. Typical force curve of an as-received Si wafer with native oxide using a Si_3N_4 tip on a cantilever with the nominal spring constant $K = 0.32$ nN/nm. The cantilever deflection difference $\Delta Z_{V(Silicon)} = 7.58$ V results from the adhesive forces.

cantilever displacement Z, is shown in Fig. 2. Initially, when the cantilever approaches the sample, the cantilever deflection is essentially zero until the tip contacts the surface [Fig. 2 (label A)]; then, the cantilever deflection signal increases linearly with the cantilever displacement. When the cantilever next is retracted [Fig. 2 (label B)] from the surface, the cantilever deflection signal decreases linearly with the cantilever displacement past point A (Fig. 2) due to adhesive forces between tip and sample until point C (Fig. 2), where the cantilever spring force exceeds the adhesive forces and the cantilever snaps off from the sample. As a result, the force distance curve shows hysteresis, which is characterized by the deflection signal difference ΔZ_V between points A and C, corresponding to the deflection difference ΔZ. The nanoscale adhesive force F_{adh} can then be calculated from the force–distance curve using the spring constant K of the AFM cantilever ($K = 0.32$ nN/nm in this paper) and a calibration constant C_{Vm} for the AFM instrument, i.e.,

$$F_{adh} = K \times \Delta Z = K \times \Delta Z_V \times C_{Vm}. \qquad (1)$$

The calibration constant is used to convert the original voltage output ΔZ_V of the AFM to the metric cantilever deflection ΔZ. The calibration constant was obtained from the force–distance curve of the same AFM tip on natural diamond. Since diamond is a very hard material, no deformation takes place when the tip is pushed against the surface. Thus, the cantilever deflection equals the piezotube displacement. The calibration constant is different for each AFM tip. In this paper, the nominal spring constant of the AFM cantilever is used. Since the spring constant may vary from one AFM cantilever to another, all the data in Fig. 6 were obtained using the same AFM cantilever, whose C_{Vm} was determined as 60 ± 8 nm/V. The calibration was done before and after the data in Fig. 6 were obtained with essentially identical results. This is important since during force calibration and adhesive force measurements, the tip shape and the contact area between the tip and the surface might change due to tip wear or contamination; therefore, the force curve on the same surface was measured regularly to see if tip wear/contamination effects appeared. If tip

TABLE I
WATER CONTACT ANGLES, SURFACE ENERGY, AND ROUGHNESS OF SAM COATINGS ON SILICON

	FDTS	FOTS	FOMDS	FOMMS	FOTES	OTS
θ_{st} (water)	115.4	111.7	112.8	110.4	103.6	100
Surface energy γ_{sv} (mJ/m^2)	9.95	10.93	11.35	11.54	14.26	25.44
γ_{sv} Dispersive component (mJ/m^2)	9.06	9.54	10.26	9.90	11.56	24.65
γ_{sv} Polar component (mJ/m^2)	0.89	1.40	1.09	1.64	2.70	0.79
R_{RMS} (nm) [a]	0.18	0.09	0.16	0.16	0.15	0.11
R_a roughness (nm) [a]	0.14	0.07	0.13	0.12	0.12	0.09

[a] R_{RMS} and R_a roughness of the silicon substrate is 0.34 and 0.28 nm respectively.

wear/contamination appeared in the measurements, the AFM cantilever was replaced. For each sample, the adhesive forces were measured in more than 20 different locations.

The AFM friction measurements were done in lateral force microscopy mode. All scans were performed in a direction that is perpendicular to the long axis of the cantilever beam with a tip velocity of 2.01 μm/s and a scan length of 1 μm. The normal load was changed at the end of each scan by adjusting the set point value. For a given load, the friction signals for both forward and backward scans were recorded. The average friction signal was taken as half the difference between the forward and backward friction signals. The friction signal can be calibrated to real friction force using a friction calibration constant for each tip. However, the calibration was not done in this paper. The relative friction coefficient was determined by measuring the friction signal as a function of AFM set points, as described in the inset of Fig. 8. For each sample, the friction forces were measured at at least three different locations. For easy comparison, all data that are presented in one plot were obtained with the same AFM tip. A detailed explanation of friction measurement can be found in [28].

The thermal stability of SAM coatings was monitored by water static contact angle measurements. The samples were annealed in air (ordinary room ambient with a relative humidity of 40% at 20 °C) on a hot plate at a predefined temperature for 2 min and then removed from the hot plate to a bulk aluminum plate and allowed to cool down to room temperature. The static water contact angle was then measured at room temperature. Afterward, the same sample was reheated at the next given temperature for 2 min and measured again. The accuracy of this approach was evaluated by measuring the transient and steady-state temperatures of a silicon wafer with embedded thermocouple (Sensarray Corporation, Santa Clara, CA) when this was placed on the hot plate to mimic the thermal treatment of the samples. This was done at all temperature settings that were used in the experiment. The thermometer wafer reached the steady-state temperature within 5 °C in less than 0.5 min. The experiments were repeated, with the thermometer wafer placed on top of a silicon sample with essentially identical results. Now, the thermometer actually measures some average cross-sectional temperature of the wafer; however, since the thermal time constant of the wafer is very short, i.e., $\tau \approx (\pi/2)^2(h^2/D_{th}) < 8$ ms, this represents the surface temperature well on the time scale that is relevant in these experiments. Here, h is the wafer thickness,

and $D_{th} \approx 0.8$ cm^2/s is the thermal diffusivity of silicon. Note also that the high thermal conductivity of silicon $\kappa \approx 150$ W/(mK) eliminates the possibility of substantial static thermal gradients in the silicon wafer. From the preceding discussion, we conclude that the temperatures that were reported in the thermal degradation experiments represent the actual surface temperature within less than 5 °C, and the effective time at high temperature is roughly the hot plate time (2 min) within less than 0.5 min.

III. RESULT AND DISCUSSION

FDTS, FOTS, FOMDS, FOMMS, FOTES, and OTS were successfully used as source materials for the deposition of SAM coatings on 4″ monosilicon (100) wafers using a vapor-phase process [26]. The static water contact angle θ_{st}, surface energy γ_{sv}, root-mean-square roughness R_{rms}, and average roughness R_a of SAM coatings without aggregations are listed in Table I. It appears that, under good deposition conditions, FDTS, FOTS, FOMDS, and FOMMS have a very high water static contact angle ($> 110°$), while OTS has a significantly lower contact angle of $100°$ due to its hydrocarbon backbone. This is not a surprise since it is already well known that fluorocarbon-based coatings have better anti-stiction properties than hydrocarbon-based coatings [10], [14], [29]. However, fluorocarbon-based coatings are also expected to have larger friction force than hydrocarbon-based coatings [30] due to the helical backbone structure of fluorocarbon chain and, thereby, larger stiffness [31], [32]. A coating grown from OTS has a larger surface energy compared to fluorocarbon-based SAM coatings due to a much larger dispersive component of its surface energy. FOTES is an ethoxysilane-based precursor, whose reactivity is much lower than that of chlorosilane. Therefore, in the deposition setup that was used for the experiments in this paper, it is very difficult to control the FOTES deposition process. The SAM coatings that were grown from FOTES thus might have lower coverage and packing density, which leads to its lower contact angle. Fig. 3 shows AFM images of the native monosilicon substrate and the six different SAM coated silicon substrates under the optimized deposition process parameters. All the AFM images were taken from the center of the wafers. There are no or only a few aggregations formed on those SAM coatings, as observed in AFM. However, wafers with many aggregations were also produced with other less appropriate process parameters where too much water was introduced into
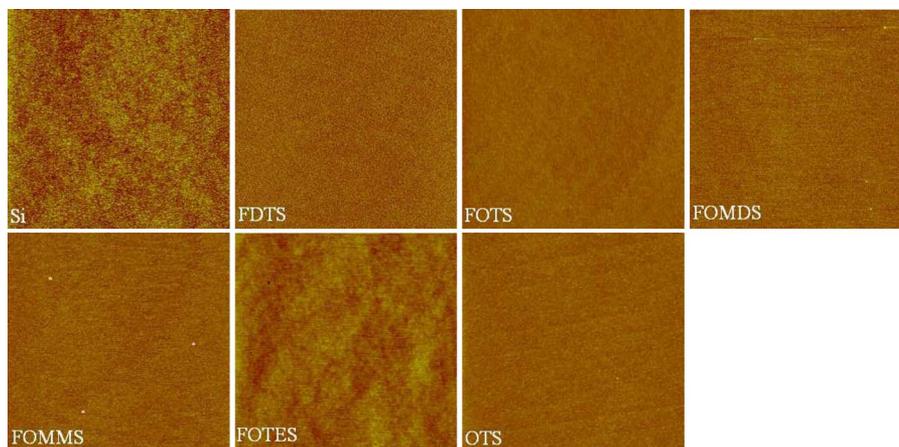
Fig. 3. AFM images for native monosilicon and various SAM-coated surfaces. There are little or no aggregations on the coatings. Note that all AFM images are shown with identical height scales in the range of 0–5 nm and scanning areas of 5×5 μm.
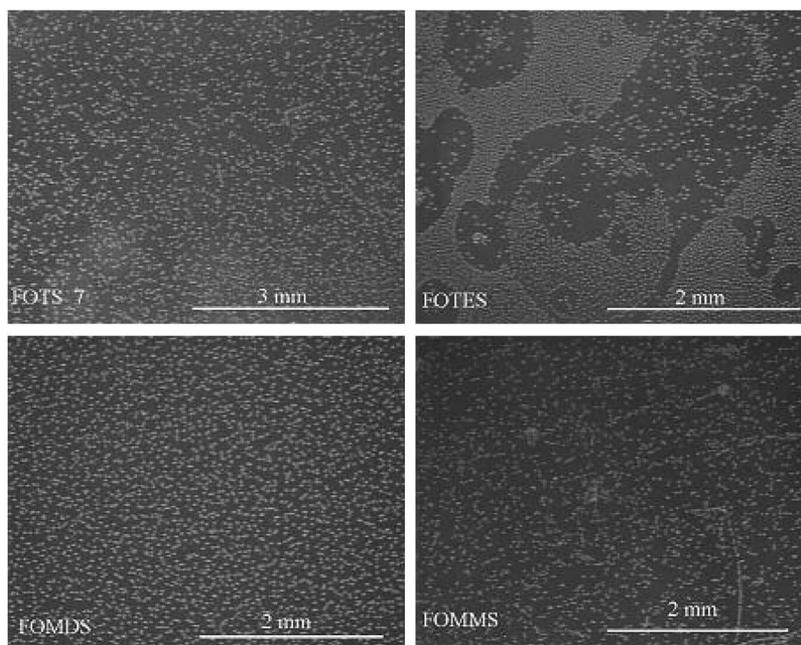

Fig. 4. Optical microphotograph of water condensation figures for SAM coatings grown from FOTS, FOTES, FOMDS, and FOMMS, respectively.

the reaction chamber during the deposition process. All the SAM coatings have slightly lower roughness than the native monosilicon substrate.

The homogeneity of the coatings was examined by water condensation figures and AFM scans on the central line that is parallel to the primary flat of wafers. Fig. 4 shows water condensation figures of SAM coatings that were grown from FOTS, FOMDS, FOMMS, and FOTES, respectively. It is observed that the water microdroplets are homogeneously distributed on FOTS and FOMDS, while clear patterns are seen on FOTES. This indicates that the coatings that were grown from FOTS and FOMDS have good homogeneity, while coatings that were grown from FOMMS and FOTES are significantly less homogeneous. We have also observed that it is very hard to get a good-quality FOTES SAM coating with the deposition setup that was used. Fig. 5 shows the rms roughness of FDTS, FOTS, FOMDS, FOMMS, and OTS SAM coatings on the central line that is parallel to the primary flat of wafer. The variation in
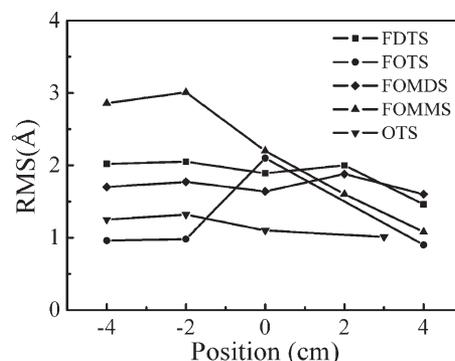

Fig. 5. RMS roughness along the central line that is parallel to the primary flat of the wafer, showing good homogeneity of the SAM coatings.

roughness across the wafer is seen to be very small in most cases; the FOMMS coating has a significant variation in the roughness, but still the roughness is small.
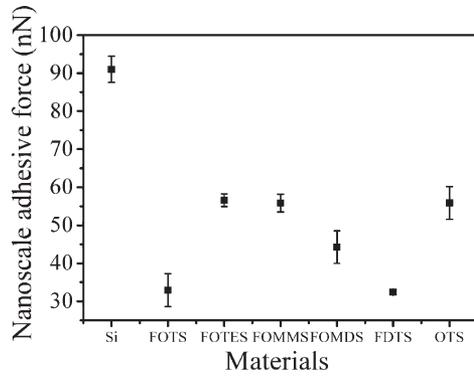
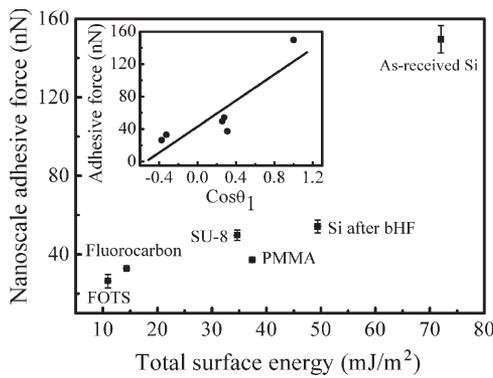Fig. 6.　Nanoscale adhesive forces of six SAM coatings and of bare silicon.

Fig. 7.　Nanoscale adhesive forces as a function of the total surface energy for several MEMS materials and a FOTS SAM coating. The inset shows the correlation between adhesive forces and the cosine of the water contact angle.
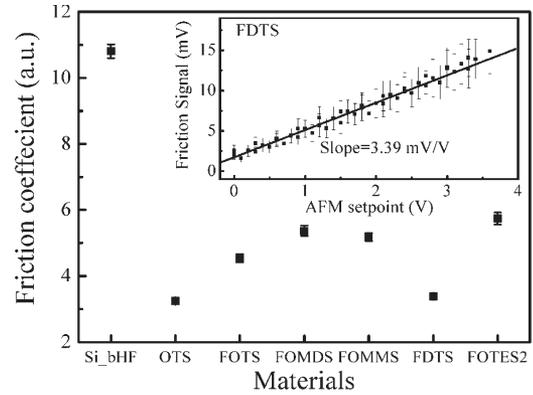

Fig. 8.　Relative friction coefficient of SAM coatings and fresh bHF-dipped silicon. The inset shows the experimental determination of the relative friction coefficient from experimental data.
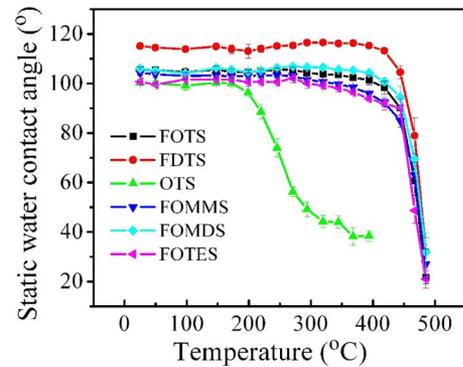

Fig. 9.　Static water contact angle of six SAM coatings as a function of annealing temperature. The annealing time was 2 min at each temperature.

Fig. 6 shows nanoscale adhesive forces between a Si_3N_4 AFM tip and the six different SAM coatings. The nanoscale adhesive force between the Si_3N_4 AFM tip and an as-received Si wafer is also given in Fig. 6. We observe that the nanoscale adhesive force of any of the SAM coatings is much smaller than that of the silicon wafer with native oxide; thus, the SAM coatings can significantly reduce stiction problems in Si microstructures. Among the SAM coatings, the adhesive force increases in the order of FDTS < FOTS < FOMDS < FOMMS < OTS < FOTES. In order to compare the adhesive force of SAM coating to other commonly used MEMS materials, the contact angle, surface energy, and adhesive force of as-received silicon, SU-8, polymethyl methacrylate (PMMA), a fluorocarbon film that was deposited by the passivation process in deep reactive ion etching (DRIE), and silicon after a buffered hydrofluoric acid (bHF) dip have been determined and plotted in Fig. 7 together with the data for a FOTS SAM coating. Please note that the AFM tip and the silicon that was used in Fig. 7 are different from those used in Fig. 6, which might explain why the measured adhesive force of silicon differs in these two figures. In Fig. 7, we see that the adhesive forces of SU-8 and PMMA are three to four times smaller than that of an as-received silicon wafer, indicating that SU-8 and PMMA have a lower tendency to stick. A bHF dip can dramatically reduce the adhesive forces of a silicon wafer since it produces an H-terminated surface. Fluorocarbon film that is

deposited in a DRIE tool has even smaller adhesive forces, while a FOTS coating has the smallest adhesive force and, thereby, an even better anti-stiction ability. Apparently, there is a correlation between surface energy and adhesive force, i.e., the materials with higher surface energies have higher adhesive forces.

In the AFM adhesion measurements, the contact between the tip and a flat sample surface is just like a sphere in contact with a flat surface [33], where the attractive Laplace force that is caused by water capillary is

$$F_L = 2\pi R \gamma_{lv}(\cos\theta_1 + \cos\theta_2) \qquad (2)$$

where R is the radius of the sphere, γ_{lv} is the surface tension of the liquid against air, and θ_1 and θ_2 are the contact angles between liquid and flat and spherical surfaces, respectively. In the AFM adhesive tests, the same AFM tip is used; thus, θ_2 can be assumed to be constant, while θ_1 is the water contact angle of materials in question. It follows that the attractive water capillary force F_L is proportional to $\cos\theta_1$. If the other interfacial forces, such as van der Waals forces, are very small compared to the capillary force, the adhesive force can be approximated by F_L; thus, the adhesive force is approximately proportional to $\cos\theta_1$. The inset in Fig. 7 shows the nanoscale

TABLE II
CONTACT ANGLE, ADHESION FORCE, FRICTION COEFFICIENT, AND THERMAL STABILITY OF THE SIX SAM COATINGS
RANKED ACCORDING TO PERFORMANCE. THE FIRST PERFORMANCE MEANS HIGHEST CONTACT ANGLE,
LOWEST ADHESION FORCE, LOWEST FRICTION COEFFICIENT, AND HIGHEST THERMAL STABILITY

Performance	Contact angle	Adhesion force	Friction coefficient	Thermal stability
1st	FDTS	FDTS	OTS	FDTS
2nd	FOTS	FOTS	FDTS	FOMDS
3rd	FOMDS	FOMDS	FOTS	FOTS
4th	FOMMS	FOMMS	FOMMS	FOMMS
5th	FOTES	OTS	FOMDS	FOTES
6th	OTS	FOTES	FOTES	OTS

adhesive force as a function of $\cos\theta_1$, verifying a strong correlation.

Fig. 8 shows the relative friction coefficient of the various materials that were investigated. The friction coefficient of fresh bHF dipped silicon is also shown in Fig. 8 as a reference. The inset in Fig. 8 shows the experimental determination of the friction coefficient from experimental data. It appears that the friction coefficient increases in the order of OTS $<$ FDTS $<$ FOTS $<$ FOMMS $<$ FOMDS $<$ FOTES $<$ Si$_{\text{bHF}}$. Bhushan and Liu suggested a molecular spring model for SAM coatings [33], where it is assumed that an AFM tip sliding on the surface of SAMs is similar to a tip sliding on the top of molecular springs or a molecular brush. The molecular spring assembly has compliant features and can experience change in orientation and compression under normal load. The orientation of the "molecular springs or brush" under normal load reduces the shearing force at the interface, which in turn reduces the friction force. The possibility of orientation is determined by the spring constant of a single molecule, as well as the interaction between the neighboring molecules, which is reflected by the packing density or packing energy. According to this model, SAM coatings have smaller friction forces compared to silicon substrates. The different friction forces of various SAM coatings can be explained by different single-molecule spring constants and different coverages of the coatings (or packing density). The backbone in OTS has a zigzag configuration, while that in the fluorinated molecules have a helical backbone. The fluorinated molecules present a larger lateral resistance to the sliding than OTS and thereby have larger friction force and friction coefficient [31]. The five fluorinated SAM coatings may have different coverage/packing densities due to different steric hindrances. Thus, the five fluorinated SAM coatings have different friction forces, even though they have the same or similar backbone configuration.

Fig. 9 shows the static water contact angle of the SAM coatings that were grown from FDTS, FOTS, OTS, FOMMS, FOMDS, and FOTES as a function of annealing temperature. The annealing time at each temperature was 2 min. The SAM coating that was grown from FDTS has the best thermal stability among the six SAM coatings; its contact angle remains unaffected by annealing in air at temperatures below approximately 405 °C. SAM coatings that were grown from OTS have the poorest thermal stability due to the hydrocarbon backbone; the water contact angle is only stable up to 175 °C. These results are in agreement with the earlier data that were reported for liquid-based FDTS [10], [34] and OTS [10], [12], [23], [34], where the liquid-based FDTS coating was found to survive in air up to 400 °C, while the OTS coatings begin to gradually degrade at about 200 °C. The degradation temperature is dependent on the coating quality since aggregations on the SAM coatings significantly reduce their thermal stability [35].

Maboudian et al. have reported on the thermal degradation behavior in vacuum of OTS [36] and FDTS [37] on oxidized surfaces. They found that OTS coatings are stable in vacuum up to 467 °C and then begin to decompose through C–C bond cleavage, while FDTS loses the fluorinated groups during annealing by the loss of the entire molecular chain. It has also been reported that the OTS has better thermal stability in N_2 than in air, while a N_2 ambient does not improve the thermal stability of FDTS [10] compared to the stability in air. This indicated that FDTS degrades through the loss of the entire molecular chains. In this paper, the thermal stability heat treatment has been performed in air, followed by a measurement of water contact angle on the coating surface. The presence of O_2 and water significantly decreases the thermal stability of OTS. The slight difference in thermal stability of the five fluorinated SAM coatings might be caused mainly by different initial coverages.

For easy comparison of the six SAM coatings, their water contact angle, nanoscale adhesive force, friction force, and thermal stability are summarized in Table II. For anti-stiction application, the coating should have high water contact angle, low adhesion force, low friction force, and high thermal stability. FDTS has the best performance with respect to contact angle, adhesion force, and thermal stability, followed by FOTS. However, both of the two coatings are formed by trichlorosilane, which produce 3HCl molecules per precursor molecule. For some sensitive devices where HCl could be a problem, FOMDS, FOMMS, or even FOTES can be used due to their quite good anti-stiction performance. OTS could be a good choice for devices demanding low friction force, reasonable anti-stiction capability, and moderate thermal stability.

IV. CONCLUSION

Six different organosilanes were used as precursors for vapor-phase growth of anti-stiction SAM coatings on silicon substrates. The contact angle, surface energy, homogeneity, roughness, nanoscale adhesive force, nanoscale friction force, and thermal stability were investigated using a contact angle

meter and AFM. The results verify good anti-stiction properties, such as high contact angle and low adhesive force for all the SAM coatings. Among the six SAM coatings, FDTS, FOMDS, and FOTS have the best anti-stiction properties when considering hydrophobization of the surface, adhesive, and friction forces, homogeneity, and thermal stability. FOMMS and FOTES are good anti-stiction precursors for applications in devices that are sensitive to HCl. OTS is useful for applications demanding low friction force.

REFERENCES

[1] R. Maboudian and R. T. Howe, "Critical review: Adhesion in surface micromechanical structures," *J. Vac. Sci. Technol. B, Microelectron. Process. Phenom.*, vol. 15, no. 1, pp. 1–20, Jan. 1997.

[2] N. Tas, T. Sonnenberg, H. Jansen, R. Legtenberg, and M. Elwenspoek, "Stiction in surface micromachining," *J. Micromech. Microeng.*, vol. 6, no. 4, pp. 385–397, 1996.

[3] K. Komvopoulos, "Adhesion and friction forces in microelectromechanical systems: Mechanisms, measurement, surface modification techniques, and adhesion theory," *J. Adhes. Sci. Technol.*, vol. 17, no. 4, pp. 477–517, 2003.

[4] C. H. Mastrangelo, "Adhesion-related failure mechanisms in micromechanical devices," *Tribol. Lett.*, vol. 3, no. 3, pp. 223–238, Sep. 1997.

[5] J. Anguita and F. Briones, "HF/H2O vapor etching of SiO2 scarificial layer for large-area surface-micromachined membranes," *Sens. Actuators A, Phys.*, vol. 64, no. 3, pp. 247–251, Jan. 1998.

[6] H. Guckel, J. J. Sniegowski, T. R. Christenson, and F. Raissi, "The application of fine-grained, tensile polysilicon to mechanically resonant transducers," *Sens. Actuators A, Phys.*, vol. 21, no. 1–3, pp. 346–351, Feb. 1990.

[7] G. T. Mulhern, D. S. Soane, and R. T. Howe, "Supercritical carbon dioxide drying of microstructures," in *Proc. 7th Int. Conf. Solid-State Sens., Actuators—Transducers*, 1993, p. 296.

[8] J. B. Brzoska, I. B. Azouz, and F. Rondelez, "Silanization of solid substrates: A step toward reproducibility," *Langmuir*, vol. 10, no. 11, pp. 4367–4373, 1994.

[9] M. Linford, R. Fenter, P. M. Eisenberger, and C. E. D. Chidsey, "Alkyl monolayers on silicon prepared from 1-alkenes and hydrogen-terminated silicon," *J. Amer. Chem. Soc.*, vol. 117, no. 11, pp. 3145–3155, Mar. 1995.

[10] U. Srinivasan, M. R. Houston, R. T. Howe, and R. Maboudian, "Alkyltricholorosilane-based self-assembled monolayer films for stiction reduction in silicon micromahines," *J. Microelectromech. Syst.*, vol. 7, no. 2, pp. 252–260, Jun. 1998.

[11] R. Maboudian, W. R. Ashurst, and C. Carraro, "Self-assembled monolayers as anti-sticiton coatings for MEMS: Characteristics and recent developments," *Sens. Actuators A, Phys.*, vol. 82, no. 1–3, pp. 219–223, May 2000.

[12] W. R. Ashurst, C. Yau, C. Carraro, R. Maboudian, and M. T. Dugger, "Dichlorodimethylsilane as an anti-stiction monolayer for MEMS: A comparison to the octadecyltrichlorosilane self-assembled monolayer," *J. Microelectromech. Syst.*, vol. 10, no. 1, pp. 41–49, Mar. 2001.

[13] B. Rarvais, A. Pallandre, A. M. Joans, and J. P. Raskin, "Liquid and vapor phase silanes coating for the release of thin film MEMS," *IEEE Trans. Device Mater. Rel.*, vol. 5, no. 2, pp. 250–254, Jun. 2005.

[14] R. Maboudian, W. R. Ashurst, and C. Carraro, "Tribological challenges in micromechanical systems," *Tribol. Lett.*, vol. 12, no. 2, pp. 95–100, Feb. 2002.

[15] S. Hozumi, K. Ushiyama, H. Sugimura, and O. Takai, "Fluoroalkylsilane monolayers formed by chemical vapor surface modification on hydroxylated oxide surfaces," *Langmuir*, vol. 15, no. 22, pp. 7600–7604, Oct. 1999.

[16] T. M. Mayer, M. P. de Boer, N. D. Shinn, P. J. Clews, and T. A. Michalske, "Chemical vapor deposition of fluoroalkylsilane monolayer films for adhesion control in microelectromechanical systems," *J. Vac. Sci. Technol. B, Microelectron. Process. Phenom.*, vol. 18, no. 5, pp. 2433–2439, Sep. 2000.

[17] M. R. Kosur, H. Gerung, Q. Li, and S. M. Han, "Vapor-phase adsorption kinetics of 1-decene on H-terminated Si(100)," *Langmuir*, vol. 19, no. 22, pp. 9315–9320, 2003.

[18] A. Hozumi, Y. Yokogawa, T. Kameyama, H. Sugimura, K. Hayashi, H. Shirayama, and O. Takai, "Amino-terminated self-assembled monolayer on a SiO2 surface formed by chemical vapor deposition," *J. Vac. Sci. Technol. A, Vac. Surf. Films*, vol. 19, no. 4, pp. 1812–1816, Jul. 2001.

[19] M. G. Hankins, P. J. Resnick, P. J. Clews, T. M. Mayer, D. R. Wheeler, D. M. Tanner, and R. A. Plass, "Vapor deposition of amino-functionalized self-assembled monolayers on MEMS," *Proc. SPIE*, vol. 4980, pp. 238–247, 2003.

[20] W. R. Ashurst, C. Carraro, and R. Maboudian, "Vapor phase anti-stiction coatings for MEMS," *IEEE Trans. Devices Mater. Rel.*, vol. 3, no. 4, pp. 173–178, Dec. 2003.

[21] W. R. Ashurst, C. Carraro, J. D. Chinn, V. Fuentes, B. Kobrin, R. Maboudian, R. Nawak, and R. Yi, "Improved vapor-phase deposition technique for anti-stiction monolayers," *Proc. SPIE*, vol. 5342, pp. 204–211, 2004.

[22] B. Kobrin, J. Chinn, R. W. Ashurst, and R. Maboudian, "Molecular vapor deposition (MVD) for improved SAM coatings," *Proc. SPIE*, vol. 5716, pp. 151–157, 2005.

[23] W. R. Ashurst, C. Carraro, M. Maboudian, and W. Frey, "Wafer level anti-stiction coatings for MEMS," *Sens. Actuators A, Phys.*, vol. 104, no. 3, pp. 213–221, May 2003.

[24] M. P. de Boer and T. M. Mayer, "Tribology of MEMS," *MRS Bull.*, vol. 26, no. 4, pp. 302–304, Apr. 2001.

[25] A. Y. Fadeev and T. J. McCarthy, "Self-assembly is not the only reaction possible between alkyltrichlorosilanes and surfaces: Monomolecular and oligomeric covalently attached layers of dichloro- and trichloroalkylsilanes on silicon," *Langmuir*, vol. 16, no. 18, pp. 7268–7274, Sep. 2000.

[26] T. Knieling, W. Lang, and W. Benecke, "Gas phase hydrophobisation of MEMS silicon structures with self-assembling monolayers for avoding in-use sticking," *Sens. Actuators B, Chem.* [Online]. Available: doi:10.1016/j.snb.2006.10.023

[27] Y. X. Zhuang and A. Menon, "Wettability and thermal stability of fluorocarbon films deposited by deep reactive ion etching," *J. Vac. Sci. Technol. A, Vac. Surf. Films*, vol. 23, no. 3, pp. 434–439, May 2005.

[28] B. Bhushan, *Handbook of Nanotechnology*. Heidelberg, Germany: Springer-Verlag, 2004.

[29] R. Banga, J. Rarwood, A. M. Morgan, and B. Evans, "FTIR and AFM studies of the kinetics and self-assembly of alkyltrichlorosilane and (perfluoroalkyl) trichlorosilanes onto glass and silicon," *Langmuir*, vol. 11, no. 11, pp. 4393–4399, Nov. 1995.

[30] H. I. Kim, T. Koini, T. R. Lee, and S. S. Perry, "Molecular contributions to the frictional properties of fluorinated self-assembled monolayers," *Tribol. Lett.*, vol. 4, no. 2, pp. 137–140, 1998.

[31] O. P. Khatri, D. Devaprakasam, and S. K. Biswas, "Frictional responses of Octadecyltrichlorosilane (OTS) and 1H, 1H, 2H, 2H-perfluorooctyltrichlorosilane (FOTS) monolayers self-assembled on aluminium over six orders of contact length scale," *Tribol. Lett.*, vol. 20, no. 3/4, pp. 235–246, Dec. 2005.

[32] C. D. Lorenz, E. B. Webb, III, M. J. Stevens, M. Chandross, and G. S. Grest, "Frictional dynamics of perfluorinated self-assembled monolayers on amorphous SiO2," *Tribol. Lett.*, vol. 19, no. 2, pp. 93–99, Jun. 2005.

[33] B. Bhushan and H. Liu, "Nanotribological properties and mechanisms of alkylthiol and biphenyl thiol self-assembled monolayers studied by AFM," *Phys. Rev.*, vol. 63, no. 24, p. 245 412, Jun. 2001.

[34] B. H. Kim, T. D. Chuang, C. H. Oh, and K. Chun, "A new organic modifier for anti-stiction," *J. Microelectromech. Syst.*, vol. 10, no. 1, pp. 33–40, Mar. 2001.

[35] Y. X. Zhuang, O. Hansen, T. Knieling, C. Wang, P. Rombach, W. Lang, W. Benecke, M. Kehlenbeck, and J. Koblitz, "Thermal stability of vapor phase deposited self-assembled monolayers for MEMS anti-stiction," *J. Micromech. Microeng.*, vol. 16, no. 11, pp. 2259–2264, Nov. 2006.

[36] G. J. Kluth, M. M. Sung, and R. Maboudian, "Thermal behavior of alkyl-siloxane self-assembled monolayers on the oxidized Si(100) surface," *Langmuir*, vol. 13, no. 14, pp. 3775–3780, Jul. 1997.

[37] J. Fréchette, R. Maboudian, and C. Carraro, "Thermal behaviour of perfluoroalkylsiloxane monolayers on the oxidized Si(100) surface," *Langmuir*, vol. 22, no. 6, pp. 2726–2730, Mar. 2006.

Yan Xin Zhuang received the B.S. degree in metallurgy from Northeastern University, Shenyang, China, in 1992, and the Ph.D. degree in materials science and engineering from the Institute of Metal, Chinese Academy of Science, Beijing, China, in 1998.

From 1998 to 2002, she was a Postdoctoral Fellow with the Institute of Physics, Chinese Academy of Science, and with the Department of Physics, Technical University of Denmark, Lyngby, Denmark. Since 2003, she has been with the Center for Individual Nanoparticle Functionality, MIC–Department of Micro and Nanotechnology, Technical University of Denmark. Her research topics include anti-stiction coating for MEMS, self-assembled monolayer, metallic glasses, and micro and nanotechnology.

Pirmin Rombach received the M.Sc. degree in electronics engineering from the Technical University of Karlsruhe, Karlsruhe, Germany, in 1989, and the Ph.D. degree in electronics engineering, for his work on a micromachined torque sensor, from the Technical University of Darmstadt, Darmstadt, Germany, in 1995.

He was a Research Assistant in the Solid-State Electronics Laboratory, Technical University of Darmstadt. In 1996, he joined the research group of Microtronic (currently Sonion MEMS A/S), Roskilde, Denmark. The focus of his research has been modeling and process development for micromachined microphones and loudspeakers and also packaging for microsystems, especially for silicon microphones. Since 2003, he has been the Head of R&D at Sonion MEMS A/S, being responsible for the product development of silicon microphones, which have been commercially available since 2005. In July 2007, he temporarily joined Sonion Vietnam, Ho Chi Minh City, Vietnam, for a technology transfer project to start up the production in Sonion's production facility.

Ole Hansen was born in Sorø, Denmark, on February 11, 1951. He received the M.Sc. degree from the Technical University of Denmark, Lyngby, Denmark, in 1977.

Since 1990, he has been an Associate Professor with MIC–Department of Micro and Nanotechnology, Technical University of Denmark. Since 2005, he has also been a part of the Danish National Research Foundation's Center for Individual Nanoparticle Functionality, MIC–Department of Micro and Nanotechnology. He has conducted research in the areas of semiconductor devices, silicon fabrication technology, MEMS, and NEMS. Currently, his main effort is devoted to fundamental studies of catalytic activity of nanoparticles using a combination of surface science tools and micro and nanofabricated reactors. He is presently teaching three lecture courses: semiconductor technology, semiconductor devices, and microelectromechanical systems.

Walter Lang received the Diploma in physics, with a focus on Raman spectroscopy of crystals with low symmetry from Munich University, Munich, Germany, in 1982, and the Ph.D. degree in engineering, with a focus on flame-induced vibrations, from Munich Technical University, Munich.

In 1987, he joined the Fraunhofer Institute for Solid State Technology, Munich, where he worked on microsystems technology. In 1995, he became the Head of the Sensors Department, Institute of Micromachining and Information Technology, Hahn-Schickard Gesellschaft, Villingen-Schwenningen, Germany, working on microsensors for flow, angular rate and inclination, sensor test, and modeling. In February 2003, he joined the University of Bremen, Bremen, Germany, where together with Prof. W. Benecke, he is heading the Institute for Microsensors, -Actuators and -Systems. His current areas of sensor and technology research are microfluidic systems, flow sensors, microphones, and microanalysis systems. In the systems field, he is investigating autonomous sensor networks for logistics.

Thomas Knieling was born in Homberg/Efze, Germany, on July 23, 1968. He received the Diploma in physics from the University of Göttingen/Max Planck Institute (MPI) for Flow Research (currently MPI for Dynamics und Self-Organization), Göttingen, Germany, in 2001, and the Ph.D. degree in electrical engineering from the Institute for Microsensors, -Actuators, and -Systems, University of Bremen, Bremen, Germany, in 2007.

Since 2006, he has been with the Fraunhofer Institute for Photonic Microsystems, Dresden, Germany, working on research and development of microscanning mirrors and on speckle reduction in laser projection displays.

Wolfgang Benecke was born in Germany in 1953. He received the Dipl. Phys. degree from the Technical University of Clausthal, Clausthal-Zellerfeld, Germany, and the Ph.D. degree in material science in 1982 from the Technical University of Berlin, Berlin, Germany.

From 1984 to 1992, he was with the Fraunhofer Institute, Berlin, as the Head of the Department for Micromechanics and MEMS. Since 1992, he has been a Full Professor with the University of Bremen, Bremen, Germany, where he founded the Institute for Microsensors, -Actuators and -Systems (IMSAS). IMSAS works on MEMS covering the spectrum from conception to realization, with focus on technological aspects around silicon-based systems. Applications are in the medical, automotive, and environmental sensing fields. IMSAS operates state-of-the-art clean room facilities for the realization of MEMS devices. He is a member of the MicroSystemsCenter Bremen and Embedded Microsystems Bremen GmbH and a cofounder of microFAB Bremen GmbH, a company offering technology services for MEMS fabrication. He is a member of the editorial board of *Sensors and Actuators A: Physical*.

Prof. Benecke was the General Chairman of the 11th Annual International IEEE Workshop on Micro Electro Mechanical Systems (MEMS'92) and the German-American Frontiers of Engineers (GAFOE) Workshop in 2000 and a Committee Member of the German-American Academic Council. He is a member of the Technical Program Committee of the EUROSENSORS Conference.

Christian Wang received the M.Sc. degree in chemistry from Copenhagen University, Copenhagen, Denmark, in 1996.

Since 2000, he has been with Sonion MEMS A/S (formerly Microtronic), Roskilde, Denmark, working on anti-stiction coatings for silicon microphones. His areas of interest include MEMS packaging, electronic materials, and surface and solder joint technology.

Markus Kehlenbeck was born in Bremen, Germany, in 1971. He received the Dipl. Ing. degree in engineering from the Technical University of Braunschweig, Braunschweig, Germany.

From 1999 to 2001, he was with Tissuse GmbH, a spin-off company of the University of Leipzig, Leipzig, Germany, with core competence in microreactor design for mammalian cells. From 2001 to 2002, he was an External Construction Engineer within a development project by the Evotec OAI company, which is a large supplier of biochemical analyses and a manufacturer of automatic analysis machines with nanosized probe volumes. From 2002 to 2005, he was a Process Engineer and then a Project Engineer with microFAB Bremen GmbH, which is an industrial MEMS supplier and produces silicon-based MEMS in a clean room facility in Bremen, Germany. Since 2006, he has been with the Industrial Engineering Department, Hella Fahrzeugkomponenten GmbH, Bremen, a member of the Hella Group that is a sensor and actuator supplier for the automotive industry.

Jörn Koblitz was born in Hamburg, Germany, on June 21, 1961. He received the Bachelor's degree in engineering from the Technical University of Osnabrück, Osnabrück, Germany, in 1987.

From 1987 to 1990, he was a Process Engineer with Philips Semiconductor, Hamburg, Germany. From 1994 to 2001, he was a Facility Manager at the Institute of Microsensors, -Actuators, and -Systems, University of Bremen, Germany. He is currently the Managing Director and cofounder of microFAB Bremen GmbH, Bremen, a MEMS silicon wafer foundry.